Mon. Not. R. Astron. Soc. **000**, 1–7 (2005) Printed 6 March 2006 (MN LATEX style file v2.2)

1.4 GHz polarimetric observations of the two fields imaged by the DASI experiment

G. Bernardi[1⋆], E. Carretti[1], R.J. Sault[2], S. Cortiglioni[1] and S. Poppi[3]
[1] *INAF–IASF Bologna, Via Gobetti 101, Bologna, I-40129, Italy*
[2] *CSIRO–ATNF, P.O. Box 76, Epping, NSW 1710, Australia*
[3] *INAF–IRA Bologna, Via Gobetti 101, Bologna, I-40129, Italy*

Accepted xx xx xx. Received yy yy yy; in original form zz zz zz

ABSTRACT

We present results of polarization observations at 1.4 GHz of the two fields imaged by the DASI experiment ($\alpha = 23^{\rm h}30^{\rm m}$, $\delta = -55°$ and $\alpha = 00^{\rm h}30^{\rm m}$, $\delta = -55°$, respectively). Data were taken with the Australia Telescope Compact Array with 3.4 arcmin resolution and ~ 0.18 mJy beam^{-1} sensitivity. The emission is dominated by point sources and we do not find evidence for diffuse synchrotron radiation even after source subtraction. This allows to estimate an upper limit of the diffuse polarized emission. The extrapolation to 30 GHz suggests that the synchrotron radiation is lower than the polarized signal measured by the DASI experiment by at least 2 orders of magnitude. This further supports the conclusions drawn by the DASI team itself about the negligible Galactic foreground contamination in their data set, improving by a factor ~ 5 the upper limit estimated by Leitch et al. (2005).

The dominant point source emission allows us to estimate the contamination of the CMB by extragalactic foregrounds. We computed the power spectrum of their contribution and its extrapolation to 30 GHz provides a framework where the CMB signal should dominate. However, our results do not match the conclusions of the DASI team about the negligibility of point source contamination, suggesting to take into account a source subtraction from the DASI data.

Key words: cosmology: cosmic microwave background – polarization – radio continuum: ISM – diffuse radiation – radiation mechanisms: non-thermal.

1 INTRODUCTION

The key role played by the Cosmic Microwave Background Polarization (CMBP) in modern cosmology is now well established. The CMB E–mode carries information on the reionization (e.g. Zaldarriaga 1997) and, joined to the temperature anisotropies, helps constraining the cosmological parameter estimation (e.g. Zaldarriaga, Spergel & Seljak 1997). The CMB B–mode looks interesting for its connection with the inflationary era (e.g. Kosowsky 1999) and its capability to measure the amount of primordial gravitational waves.

On the experimental hand, the search for the CMBP is under way. Detections have been claimed by the DASI (Leitch et al. 2005), CAPMAP (Barkats et al. 2004), CBI (Readhead et al. 2004) and BOOMERanG (Montroy et al. 2005) teams. However, we are far from a complete characterization of the E–mode power spectrum whereas the B–mode detection is still missing.

⋆ E-mail: bernardi@iasfbo.inaf.it

The tiny level of the CMB polarized components makes the contamination by foreground astrophysical sources even more severe than for the anisotropy temperature term.

At frequencies lower than 100 GHz, the foreground contribution is expected to be dominated by both the Galactic synchrotron emission and extragalactic radiosources.

Several theoretical works (Mesa et al. 2002, Tucci et al. 2004, de Zotti et al. 2005) studied the contamination due to point source emission on the microwave background using data coming from low frequencies surveys. In particular Mesa et al. (2002) and Tucci et al. (2004) achieve similar results pointing out that the contamination to the CMB E–mode is not serious in the 70–100 GHz frequency range. However, both of them find that extragalactic sources could be a considerable contaminant up to 44 GHz. In addition, observational efforts are underway in order to establish the properties of the radio sources directly at high frequency. The results from 18 GHz observations of the Kuhr sample (Ricci et al. 2004a) and preliminary results from a 18 GHz survey by Ricci et al. (2004b) show a substantial agreement with the predictions by Mesa et al. (2002). Given this, the

estimate of the E–mode contamination by point sources is still open for frequencies up to 44 GHz.

About the Galactic synchrotron emission, template maps (e.g. Giardino et al. 2002, Bernardi et al. 2004) suggest that the CMBP E–mode signal should be higher than the synchrotron emission on large angular scales and for frequencies around 90 GHz.

On degree and sub–degree scales, polarization observations of the diffuse synchrotron radiation in selected low emission regions have just recently begun with the aim of estimating the possible contamination on the CMBP. The field imaged by the BOOMERanG experiment was observed with both the Australia Telescope Compact Array (ATCA) at 1.4 GHz (Bernardi et al. 2003, hereafter B03, Carretti et al. 2005a) and the Parkes telescope at 2.3 GHz (Carretti et al. 2005b) providing the first characterization of the diffuse radiation in a low emission area. They find that the Galactic signal should not prevent the detection of the CMB E–mode in that area at frequencies $\geqslant 30$ GHz. A similar analysis has been conducted in another area in the Northern sky providing similar conclusions (Carretti et al. 2006). Although these results can be used as indicators of conditions in low emission regions, every area has its own specific features and requires dedicated observations, especially if representing a target for CMBP experiments.

Among the sky regions imaged by CMB experiments, direct observations of the synchrotron emission only exist for BOOMERanG area (B03) to date. Barkats et al. (2005) assessed that the CAPMAP field is not contamined at 90 GHz since they checked that the total intensity synchrotron emission in their area is below the detected polarized signal. On the other hand, DASI and CBI operated at ~ 30 GHz, where the synchrotron emission can still play a relevant role. In particular, the DASI team itself pointed out that no polarization observations are available for the two sky patches they observed (Kovac et al. 2002).

In this paper we present results of the first deep polarization observations of the two fields imaged by the DASI experiment at a frequency of 1.4 GHz, where the synchrotron emission is dominant.

The paper is organized as follows: in Section 2 we describe the observations while in Section 3 we present the power spectrum analysis. Finally, in Section 4 we discuss the results in the framework of CMBP measurements.

2 OBSERVATIONS AND RESULTS

Observations of the two DASI fields (hereafter named field 1 and field 2, see Table 1 for their coordinates) were performed in July 2003 and September 2004 with the ATCA. The EW214 configuration was used to sample the spatial frequencies between 3 and 30 arcmin. Each field has a $3^\circ \times 3^\circ$ size and the same amount of time (~ 72 h) was spent in each of them. A sensitivity of ~ 0.18 mJy/beam has been achieved in both fields in the inner $2^\circ \times 2^\circ$ square, corresponding to ~ 3.2 mK. Both of them were observed with the same system configuration whose characteristics are reported in Table 1. A standard procedure for the ATCA data reduction, as described in B03, was followed to obtain Stokes I, Q, U, V images.

Figure 1 and 2 show the results for the field 1 and 2, respectively. It is evident that the cleaning procedure did not manage to remove completely the side lobes for the brightest sources even in polarization.

Table 1. Main characteristics of the observations.

Central Frequency	1380 MHz
Effective Bandwidth	205 MHz
Field 1 (J2000)	$\alpha = 23^{\rm h}30^{\rm m}$, $\delta = -55^\circ$
Field 2 (J2000)	$\alpha = 00^{\rm h}30^{\rm m}$, $\delta = -55^\circ$
Area size for each field	$2^\circ \times 2^\circ$
Sensitivity (flux)	0.18 mJy beam^{-1}
Sensitivity (temperature)	3.2 mK
Gain	17.3 K/Jy beam^{-1}

The emission is dominated by point sources both in total intensity and polarization. Besides this, no evident diffuse polarized emission rises up the noise level in both fields. This is in contrast with that found in the B03 area observed with the same array (same configuration and sensitivity). In order to make this contrast evident, we plot the map of the Stokes parameter U measured in the B03 field for a direct comparison in Figure 1 and 2 (similar results hold for the Q images). All the structures present in the DASI fields seem to be associated to point-like sources and no extended structures are evident like in the B03 field, where a polarized diffuse emission of ~ 11 mK was detected spread throughout the area. Besides intrinsic differences due to different sky positions, the lower emission found there has been explained by the action of Faraday effects. These, by transferring power from large to small angular scales, enhance the polarized emission on the 3–30 arcmin scales the observations are sensitive to (Carretti et al. 2005b).

The DASI fields, however, are at higher Galactic latitudes ($b \sim -58^\circ$ and $b \sim -62^\circ$ for the two areas, respectively) and Carretti et al. (2005a) found that the emission is unlikely to be affected by Faraday rotation effects at 1.4 GHz at $|b| \geqslant 50^\circ$. This seems to be confirmed also by the recent polarization map at 1.4 GHz of the Northern Celestial Hemisphere (Wolleben et al. 2005).

We identify the point sources present in the two fields by setting a detection threshold of 10σ in order to avoid false and spurious candidates due to the presence of residual non–white noise. The analysis provides a catalogue complete down to a polarized flux $I_p = 2$ mJy (see Table 2 and Table 3).

We look for counterparts and find that every source, but the number six of field 1, has a radio counterpart in the Parkes survey at 408 MHz (PKS, Wright 1994), in the Parkes–MIT–NRAO survey at 4.85 GHz (PMN, Griffith & Wright 1993) or in the Sydney University Molonglo Sky Survey at 843 MHz (SUMSS, Mauch et al. 2003). In the case of source number six we find a counterpart in the optical/infrared Automated Plate Measuring survey (APM, Maddox et al. 1990). When a source is present in more than one survey, the strongest one within the beam area is listed.

Actually, we cannot justify the absence of the source number six in the field 1 in the SUMSS survey. In fact, if we consider a power law behaviour for the flux density $F_\nu \propto \nu^{\alpha_\nu}$ as a function of the frequency ν and assume a spectral index $\alpha_\nu = -0.7$, this source would have a flux of ~ 195 mJy at 843 MHz whereas the sensitivity of the SUMSS is 8 mJy.

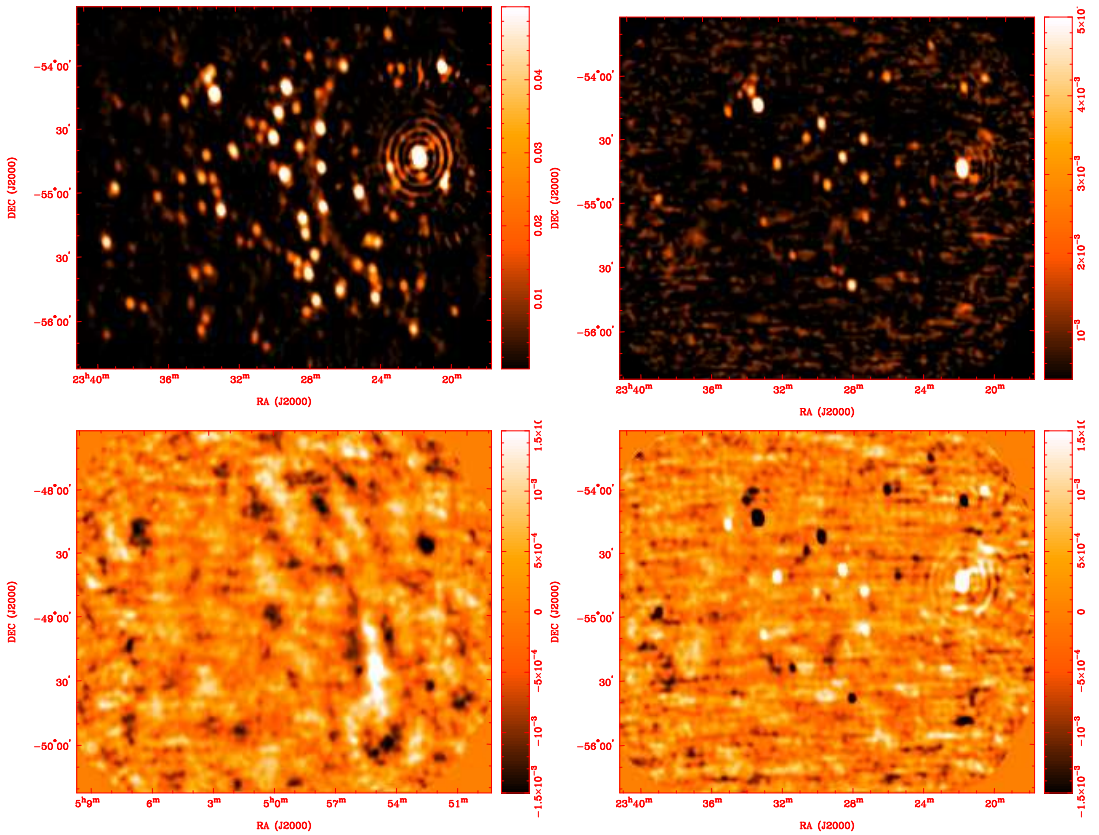

Figure 1. DASI field 1: total intensity I (top-left), polarized intensity $I^p = \sqrt{Q^2 + U^2}$ (top-right). The U image (bottom-right) is also reported for comparison with the diffuse emission (point sources subtracted) detected in B03 (bottom-left).

Even in the case of a source fully self-absorbed, the spectral index would be $\alpha_\nu = 2.5$ and the flux at 843 MHz would be ~ 40 mJy, at the limit of a 5σ detection in the SUMSS. It is worth noting that the source is unlikely to be in a complete self–absorbed regime because of its polarized emission; then the spectral slope should be flatter.

Given the limited sample, no general conclusion can be drawn but just a few qualitative remarks. We note that there are almost the same number of sources in the two fields (18 and 15, respectively) at the flux limit $I_p = 2$ mJy and almost all the sources show a polarization degree of a few per cent whereas only three sources are more than 10% polarized. The mean polarization percentage is 6.2% for the first field and 3.8% for the second one.

3 POWER SPECTRUM ANALYSIS

We compute the power spectra of the E– and B–modes in the inner $2^\circ \times 2^\circ$ square of both fields, where the sensitivity is higher. The power spectra are plotted in Figure 3 together with the noise contribution defined by (Tegmark 1997)

$$C_\ell^{noise} = \frac{f_{sky}\, 4\pi\sigma_P^2}{N\, B_\ell^2} \qquad (1)$$

where f_{sky} is the sky fraction, N is the number of pixels, B_ℓ^2 is the power spectrum of the beam–window function and σ_P the pixel sensitivity.

The power spectra fit the power law equation

Table 4. Fit parameters for E and B spectra plotted in Figure 3. The fit has been performed in the $800 < \ell < 2800$ multipole range.

Spectrum	# Field	C_{2000}^X (μK^2)	β_X
C_ℓ^E	1	183 ± 9	-0.19 ± 0.15
C_ℓ^B	1	177 ± 9	-0.44 ± 0.13
C_ℓ^E	2	345 ± 17	-0.20 ± 0.10
C_ℓ^B	2	340 ± 16	$+0.34 \pm 0.16$

$$C_\ell^X = C_{2000}^X \left(\frac{\ell}{2000}\right)^{\beta_X}, \quad X = E,\, B \qquad (2)$$

as a function of the multipole ℓ. Best fit parameters are shown in Table 4. The slopes of the spectra for the field 2 are compatible with a flat $\beta = 0$ spectrum within 2σ C.L., which is typical of the emission dominated by point sources. A similar result holds for the E–mode of the field 1, whereas the B–mode looks steeper and compatible with a point source power spectrum only at $\sim 3\sigma$ C.L. Also the spectra, therefore, support an emission dominated by point sources.

To estimate an upper limit of the diffuse emission contribution, we subtracted all the bright sources listed in Table 2 and 3. The resulting power spectra are shown in Figure 4.

It can be seen a remarkable lowering of the flux and a certain steepening of the slopes, in particular for field 2. This is clearly shown by the best fit parameters quoted in Table 5.

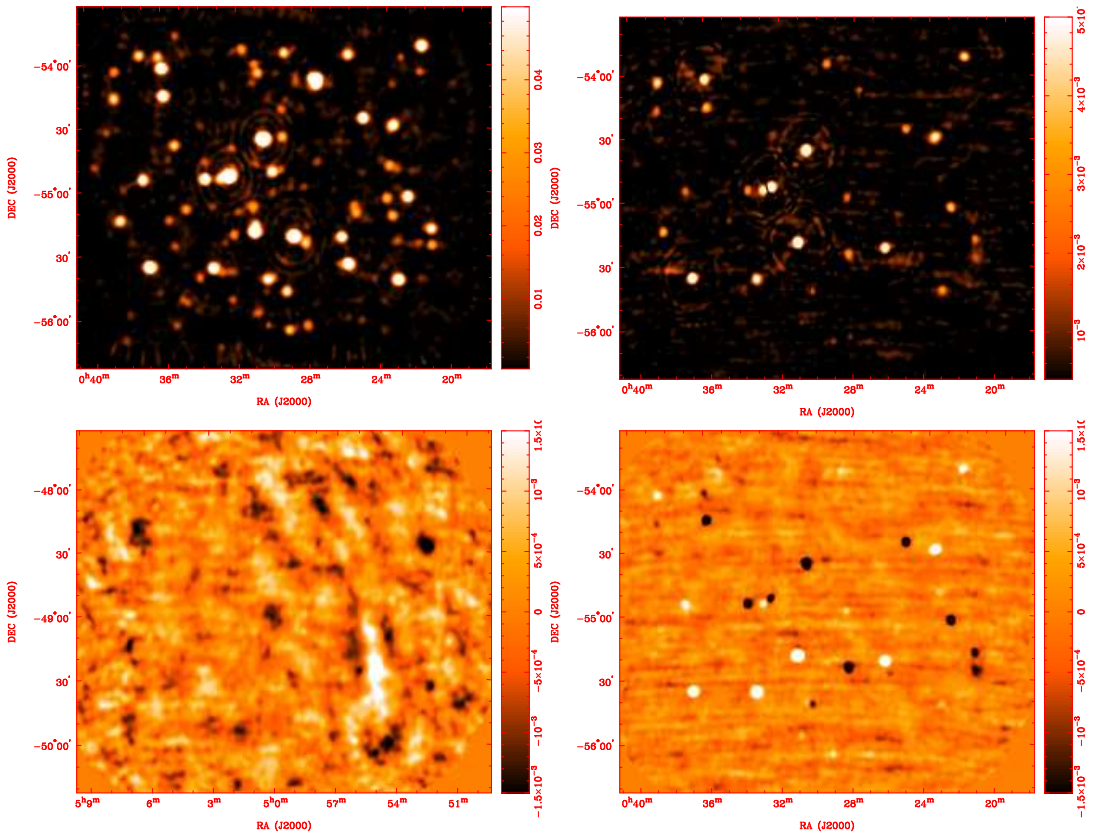

Figure 2. The same as Figure 1 but for the field 2.

Table 2. Position, total intensity (I) and polarized intensity (I^p) of the sources detected in the first DASI field. The rms-error is the same for both the two intensities and corresponds to the beam-sensitivity (0.18 mJy beam^{-1}) but an 5% error due to accuracy has to be added. Polarization angle (ϕ) and polarization degree ($\Pi = I^p/I$) are also reported. The last column provides the distance from the counterpart.

source	RA J2000	DEC J2000	I [mJy]	I^p [mJy]	ϕ	Π	counterpart	distance [arcmin]
1	$23^h22^m07^s.1$	$-54°45'29''.1$	1914.00	50.06	$-33.9° \pm 0.1°$	2.6%	PKS 2319-55	0.0
2	$23^h33^m07^s.4$	$-54°16'12''.0$	296.10	20.76	$-38.6° \pm 0.3°$	7.0%	PKS 2330-545	0.1
3	$23^h29^m34^s.5$	$-54°25'25''.2$	125.90	6.99	$39.0° \pm 0.7°$	5.6%	SUMSS J232942-542524	1.2
4	$23^h28^m04^s.8$	$-55°41'11''.2$	99.84	6.73	$11.9° \pm 0.8°$	2.4%	SUMSS J232806-554110	0.2
5	$23^h28^m35^s.4$	$-54°41'15''.0$	55.91	6.30	$-27.6° \pm 0.8°$	11.27%	SUMSS J232835-544125	0.2
6	$23^h27^m27^s.2$	$-54°42'31''.3$	136.70	5.50	$-2.4° \pm 0.9°$	4.0%	APMUKS(BJ) B232445.84-545734.8	1.7
7	$23^h33^m29^s.3$	$-54°09'25''.4$	57.30	4.76	$-10.2° \pm 1.1°$	8.3%	SUMSS J233329-540934	0.1
8	$23^h27^m24^s.8$	$-54°51'01''.0$	105.60	4.45	$-26.5° \pm 1.2°$	4.2%	SUMSS J232724-545114	0.2
9	$23^h29^m25^s.4$	$-54°54'22''.5$	209.00	4.31	$-8.7° \pm 1.2°$	2.1%	SUMSS J232925-545434	0.2
10	$23^h32^m07^s.6$	$-54°44'06''.1$	63.00	4.27	$35.0° \pm 1.2°$	6.8%	SUMSS J233207-544406	0.1
11	$23^h26^m14^s.4$	$-54°03'07''.7$	57.60	3.70	$-22.3° \pm 1.4°$	6.4%	SUMSS J232614-540321	0.2
12	$23^h30^m33^s.1$	$-54°32'06''.4$	24.02	3.63	$14.3° \pm 1.4°$	15.0%	SUMSS J233033-543141	0.4
13	$23^h34^m44^s.3$	$-54°19'00''.7$	43.37	3.32	$34.2° \pm 1.6°$	7.7%	SUMSS J233445-541910	0.2
14	$23^h27^m20^s.3$	$-55°09'16''.9$	104.20	2.86	$-31.6° \pm 1.8°$	2.7%	SUMSS J232718-550936	0.5
15	$23^h31^m20^s.1$	$-55°27'06''.4$	12.84	2.67	$-26.3° \pm 1.9°$	20.8%	SUMSS J233119-552702	0.1
16	$23^h32^m53^s.9$	$-55°11'16''.2$	106.10	2.31	$-34.5° \pm 2.2°$	2.2%	SUMSS J233253-551055	0.4
17	$23^h25^m20^s.1$	$-55°02'17''.5$	148.20	2.21	$6.5° \pm 2.3°$	1.5%	SUMSS J232520-550228	0.2
18	$23^h34^m05^s.1$	$-54°11'00''.6$	131.20	2.13	$25.3° \pm 2.4°$	1.6%	SUMSS J233404-541058	0.0

Table 3. As for Table 2 but for field 2

source	RA J2000	DEC J2000	I [mJy]	I^p [mJy]	ϕ	Π	counterpart	distance [arcmin]
1	$00^h31^m02^s.8$	$-55°21'12''.5$	264.10	15.66	$26.0° \pm 0.3°$	5.9%	PKS 0028-556	0.1
2	$00^h30^m33^s.6$	$-54°38'01''.2$	608.50	15.54	$-9.3° \pm 0.3°$	2.6%	PKS 0028-549	0.2
3	$00^h32^m26^s.3$	$-54°54'55''.3$	493.00	11.71	$6.1° \pm 0.4°$	2.4%	PKS 0030-552	0.2
4	$00^h36^m54^s.0$	$-55°36'28''.9$	196.90	11.25	$15.3° \pm 0.5°$	5.7%	SUMSS J003653-553632	0.1
5	$00^h26^m14^s.7$	$-55°23'38''.4$	105.50	8.51	$-21.3° \pm 0.6°$	8.1%	SUMSS J002615-552337	0.1
6	$00^h35^m57^s.3$	$-54°03'23''.0$	177.40	8.27	$-4.7° \pm 0.6°$	4.7%	SUMSS J003558-540324	0.1
7	$00^h32^m55^s.3$	$-54°56'28''.0$	1381.00	7.09	$7.6° \pm 0.7°$	0.5%	SUMSS J003254-545614	0.3
8	$00^h33^m20^s.3$	$-55°37'54''.9$	134.10	6.61	$-39.6° \pm 0.8°$	4.9%	SUMSS J003319-553757	0.1
9	$00^h23^m36^s.9$	$-54°31'13''.2$	98.59	6.26	$-15.8° \pm 0.8°$	6.3%	SUMSS J002340-543151	0.9
10	$00^h22^m40^s.9$	$-55°03'58''.4$	120.60	4.51	$-23.3° \pm 1.1°$	3.7%	SUMSS J002241-550400	0.0
11	$00^h35^m53^s.1$	$-54°16'47''.1$	146.50	4.31	$28.7° \pm 1.2°$	2.9%	SUMSS J003554-541634	0.3
12	$00^h25^m10^s.7$	$-54°27'39''.9$	131.40	3.56	$-39.1° \pm 1.5°$	2.7%	PMN J0025-5427	0.0
13	$00^h28^m15^s.2$	$-55°26'43''.6$	138.70	3.36	$-40.8° \pm 1.5°$	2.4%	SUMSS J002814-552701	0.3
14	$00^h23^m03^s.4$	$-55°42'48''.3$	159.80	3.32	$8.4° \pm 1.6°$	2.1%	PMN J0023-5542	0.3
15	$00^h33^m44^s.8$	$-54°56'24''.8$	152.70	3.23	$-37.1° \pm 1.6°$	2.1%	SUMSS J003344-545619	0.1

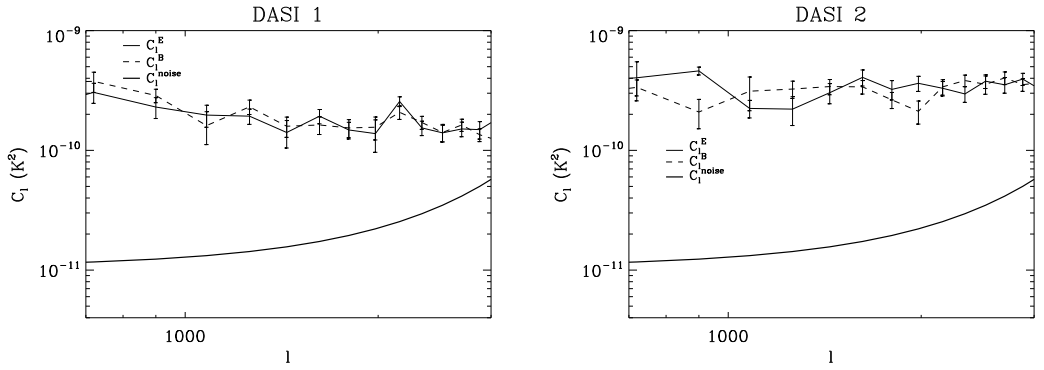

Figure 3. Power spectra of field 1 (left) and field 2 (right) with the respective 1σ error bars. Solid line represet the noise (see text).

Table 5. As for Table 4 but after point sources subtraction.

Spectrum	# Field	C_{2000}^X (μK^2)	β_X
C_ℓ^E	1	73 ± 4	-1.29 ± 0.10
C_ℓ^B	1	80 ± 4	-0.63 ± 0.13
C_ℓ^E	2	32 ± 2	-1.09 ± 0.20
C_ℓ^B	2	36 ± 3	-0.58 ± 0.25

Although these spectra certainly exhibit a lower contribution by point sources they cannot be considered as representative of the diffuse emission. In fact, the spectra match the expected noise level at the high ℓ–range tail, so that the power on the largest scales can likely be due to residual non–white noise. As a consequence, we prefer to consider these spectra as upper limits of the diffuse emission.

4 DISCUSSION

The spectra reported in Figure 3 allow an estimate of the contamination to the CMB due to point source emission. Then, we use the E–mode power spectrum (Figure 3) of the field 2, that, having the highest signal, represents the worst case. The frequency extrapolation is not trivial because of the large range of possible spectral slopes. In low frequency surveys, the radio population is a mixture of steep ($\alpha_\nu < -0.5$) and flat spectrum ($\alpha_\nu > -0.5$) sources. In particular, the steep spectrum sources have been found for the 87% of the population in the NRAO VLA Sky Survey (NVSS, Condon et al. 1998), whereas the remaining 13% are flat spectrum sources. Therefore, we take the 13% of the E–mode power spectrum and scale it up to 30 GHz with a brightness temperature spectral index $\alpha = -2.25$, which is an average value in the interval $-2.5 < \alpha < -2.0$ quoted by Toffolatti et al. (1998) for flat–spectrum sources. Then, we take the other 87% of the E–mode power spectrum and scale it up with $\alpha = -2.75$, as reported by Peacock & Gull (1981) for steep spectrum sources. The two resulting contributions are added together to give the estimate of the E–mode power spectrum at 30 GHz. Since the angular behaviour is compatible with a point source power spectrum, we extend it down to $\ell = 200$. The result is shown in Figure 5 together with the DASI measurements and the CMBP E-mode power spectrum expected according to cosmological parameters measured after WMAP data (Spergel et al. 2003).

The situation represented in Figure 5 does not exclude

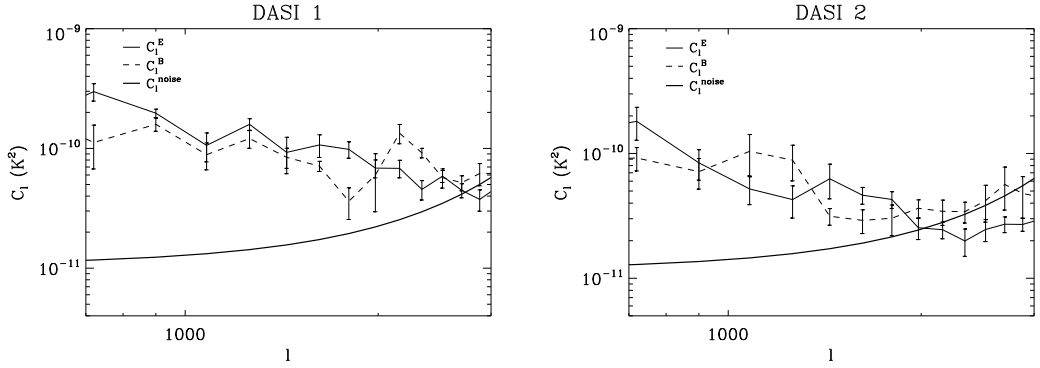

Figure 4. As for Figure3 but after point sources subtraction.

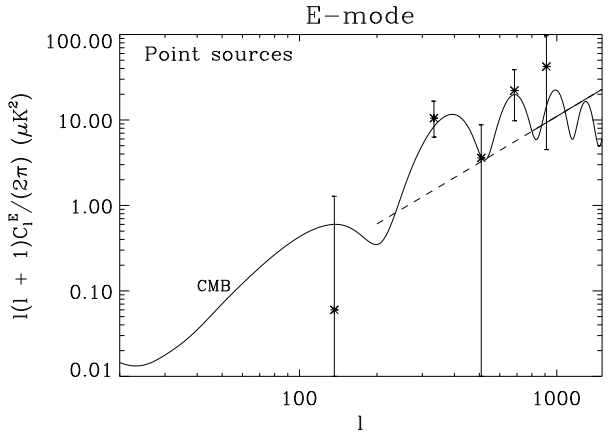

Figure 5. The CMB E–mode power spectrum (solid line) computed with the WMAP first year cosmological parameters (Spergel et al. 2003), the measurements reported by the DASI team (asterisks, Leitch et al. 2005), the extrapolation to 30 GHz of the measured power spectra in the second DASI field (solid stright line) and its extention down to $\sim 1^\circ$ angular scale (dashed line).

a point source contamination to the CMB E–mode power spectrum. At $\ell = 300$ we find $\ell(\ell+1)C_\ell^E/2\pi \simeq 1.3\ \mu\mathrm{K}^2$, which is just slightly greater than the value quoted as upper limit by Leitch et al. (2005, 0.98 $\mu\mathrm{K}^2$ at 2σ C.L.). At higher multipoles, the estimated point source emission is increasing and, compared to the CMB peaks, ranges from a factor 10 to a factor 3 lower than the CMB spectrum (3.2 and 1.7 in signal, respectively). Although within the limits of the uncertainties in the frequency extrapolation, our results suggest that the point source contamination in the DASI data is not neglibile. In the light of this, a re–analysis of the data considering a subtraction of the detected sources could allow a better estimate of the extragalactic signal component.

Power spectra of Figure 4 allow us to estimate an upper limit on the diffuse synchrotron emission as contaminant of the CMBP. We use the result of the field 1, which represents the worst case. The power spectrum of field 1 is scaled up to 30 GHz using a brightness temperature spectral index $\alpha = -3.1$ (Bernardi et al. 2004), and the result is shown in Figure 6. Since the multipole range accessible by our and DASI data are only marginally overlapped, we perform an extrapolation in the ℓ-space. Since the spectrum we measure is an upper limit and prevents us to use its slope for such extrapolation, we consider a pessimistic and a more realistic case.

We use a slope $\beta = -2.7$, that is the steepest slope measured so far for the synchrotron E-mode (Tucci et al. 2002), as a worst case. This value measured on the Galactic plane at 1.4 GHz is likely to be significantly alterated by Faraday effects. However, at the latitudes of the DASI fields, a value $\beta = -1.6 \pm 0.2$ is more likely expected (Bruscoli et al. 2002), which is more typical where Faraday rotation effects are weak. Therefore, we perform a second extrapolation using $\beta = -1.6$.

The results (Figure 6) show that the expected theoretical CMBP E-mode power spectrum is not contaminated down to the peak at $\ell \sim 300$. Considering the most likely slope of $\beta = -1.6$ we see that neither the theoretical peak at $\ell \sim 120$ would not be contamined by the synchrotron emission. The average value of the synchrotron power spectrum over the $200 < \ell < 1050$ multipole range is $\sim 0.19\ \mu\mathrm{K}^2$, which is a factor ~ 5 lower than the upper limit quoted by the DASI team (0.91 $\mu\mathrm{K}^2$, see Leitch et al. 2004). This furtherly supports the evaluation of negligible synchrotron contamination done by the DASI team itself.

In the light of the data presented in this paper, a twofold picture is emerging. Even if we did not detect the synchrotron diffuse emission at 1.4 GHz, the upper limit we set is robust enough to conclude that this component is not a serious contaminant of the CMB E–mode at 30 GHz. For this reason, our observations support the conclusions inferred by Kovac et al. (2002) and Leitch et al. (2005).

On the other hand, we argue that the problem regarding the point source contamination is still open. Leitch et al. (2005) find an upper limit of 0.98 $\mu\mathrm{K}^2$ and exclude a contamination by point sources. From the data presented here, we retrieve a value very close to it but we cannot exclude the CMBP power spectrum is not contaminated at $\ell > 300$ (Figure 5). Our data suggest the CMBP signal should dominate over the point source emission at 30 GHz but a reappraisal of the their contamination is recommended.

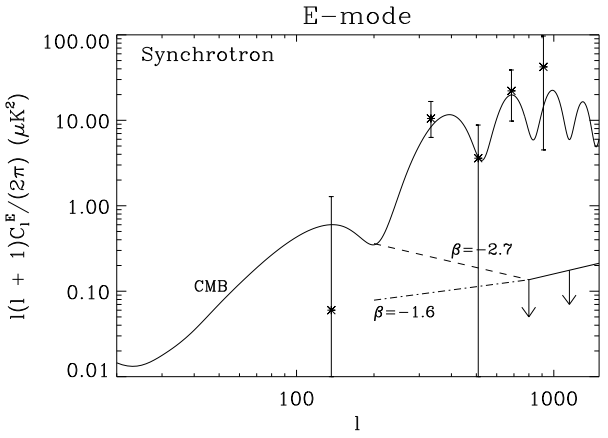

Figure 6. As Figure 5 but for the diffuse synchrotron emission: the extrapolation to 30 GHz of the upper limit on the synchrotron power spectrum obtained by our 1.4 GHz observations (solid straight line) is plotted with two possible extrapolations of the synchrotron power spectrum up to $\sim 1^\circ$ angular scale with a slope $\beta = -2.7$ (dashed line) and a slope $\beta = -1.6$ (dotted dashed line, see text for details). The arrows indicates that our extrapolation represents an upper limit.

ACKNOWLEDGMENTS

We thank Marijke Haverkorn for useful discussions and suggestions. This work has been carried out in the framework of the SPOrt experiment, a programme funded by ASI (Italian Space Agency). The Australia Telescope Compact Array is part of the Australia Telescope, which is funded by the Commonwealth of Australia for operation as a National Facility managed by CSIRO. We acknowledge the use of the CMBFAST package. This research has made use of the NASA/IPAC Extragalactic Database (NED) which is operated by the Jet Propulsion Laboratory, California Institute of Technology, under contract with the National Aeronautics and Space Administration.

REFERENCES

Barkats D., et al., 2004, ApJ, 619, L127
Bennett C.L., et al., 2003, ApJS, 148, 97
Bernardi G., Carretti E., Cortiglioni S., Sault R.J., Kesteven M.J., Poppi S., 2003 (B03), ApJ, 594, L5
Bernardi G., Carretti E., Fabbri R., Sbarra C., Cortiglioni S., Poppi S., Jonas J.L., 2004, MNRAS, 351, 436
Carretti E., Bernardi G., Sault R.J., Cortiglioni S., Poppi S., 2005a, MNRAS, 358, 1
Carretti E., McConnell D., McClure-Griffiths N.M., Bernardi G., Cortiglioni S., Poppi S., 2005b, MNRAS, 360, L10
Carretti E., Poppi S., Reich W., Reich P., Fürst E., Bernardi G. Cortiglioni S., Sbarra C., 2006, accepted for publication in MNRAS (astro–ph/0512286)
Condon J.J., Cotton W.D., Greisen E.W., Yin Q.F., Perley R.A., Taylor G.B., Broderick J.J., 1998, AJ, 115, 1693
de Zotti G., Ricci R., Mesa D., Silva L., Mazzotta P., Toffolatti L., Gonzlez-Nuevo J., 2005, A&A, 431, 893
Giardino G., Banday A.J., Górski K.M., Bennett K., Jonas J.L., Tauber J., 2002, A&A, 387, 82
Kosowsky A., 1999, New Astron. Rev., 43, 157
Kovac J. M., Leitch E. M., Pryke C., Carlstrom J. E., Halverson N. W., Holzapfel W. L., 2002, Nat, 420, 772
Leitch E.M., Kovac J.M., Halverson N.W., Carlstrom J.E., Pryke C., Smith M.W.E., 2005, ApJ, 624, 10
Maddox S.J., Sutherland W.J., Efstathiou G., Loveday J., 1990, MNRAS, 243, 692
Mauch T., Murphy T., Buttery H.J., Curran J., Hunstead R.W., Piestrzynski B., Robertson J.G., Sadler E.M., 2003, MNRAS, 342, 1117
Mesa, D. Baccigalupi C., De Zotti G., Gregorini L., Mack K.-H., Vigotti M., Klein U., 2002, A&A, 396, 463
Montroy T.E. et al., 2005, astro-ph/0507514
Peacock J.A., Gull S.F., 1981, MNRAS, 196, 611
Readhead A.C.S., et al., 2004, Science, 306, 836
Ricci R., Prandoni I., Gruppioni C., Sault R.J., De Zotti G., 2004, A&A, 415, 549
Ricci R. et al. 2004, MNRAS, 354, 305
Spergel D.N. et al., 2003, ApJ, 148, 175
Toffolatti L., Argueso Gomez F., de Zotti G., Mazzei P., Franceschini A., Danese L., Burigana C., 1998, MNRAS, 297, 117
Tucci M., Carretti E., Cecchini S., Fabbri R., Orsini M., Pierpaoli E., 2000, NewA, 5, 181
Tucci M., Carretti E., Cecchini S., Nicastro L., Fabbri R., Gaensler B.M., Dickey J.M., McClure-Griffiths N. M., 2002, ApJ, 579, 607
Tucci, M.; Martnez-Gonzlez, E.; Vielva, P.; Delabrouille, J., 2005, MNRAS in press
Wolleben M., Landecker T.L., Reich W., Wielebinski R., 2005, astro-ph/0510456
Wright A.E., 1994, AuJPh, 47, 585
Zaldarriaga M., Spergel D.N., Seljak U., 1997, ApJ, 488, 1
Zaldarriaga M., 1997, PRD, 55, 1822

This paper has been typeset from a TEX/ LATEX file prepared by the author.